H-plane SIW horn antenna with enhanced front-to-back ratio for 5G applications

Özlem AKGÜN[1],[*] , **Nurhan TÜRKER TOKAN[2]**

[1]Atatürk Strategic Studies and Graduate Institute, National Defence University, İstanbul, Turkey
[2]Department of Electronics and Communications Engineering, Faculty of Electrical & Electronics,
Yıldız Technical University, İstanbul, Turkey

Abstract: Millimeter-wave (mmWave) antennas are indispensable components in the fifth-generation (5G) wireless communication systems. With the inherent advantages of integration capability, substrate integrated waveguide (SIW) antenna is an excellent choice for applications in the mmWave frequency bands. However, reflection losses occur at dielectric-filled thin apertures of SIW antennas. These reflections can be overcome by impedance matching between the aperture and the free space. In this study, we introduce an mmWave SIW horn antenna having impedance matching transitions (IMTs) across the horn's aperture width. The designed antenna, operating in the 24–28 GHz band, is simulated with a full-wave analysis tool. The simulation results of the modified SIW horn have been confirmed by the experimental results and shown to be satisfactory. The IMTs result in an enhancement of the front-to-back ratio (FTBR). The modified SIW horn antenna with a novel printed transition achieves sidelobe levels (SLLs) of better than –9 dB at 27 GHz, with an enhanced FTBR above 15 dB. In the 24–28 GHz band, the antenna has a reflection coefficient variation of better than –10 dB.

Key words: Millimeter-wave antennas, substrate integrated waveguide, horn antenna, impedance matching, printed transitions, front-to-back ratio

1. Introduction

To meet the increasing demand for cellular communication systems, 5G networks have now become an essential technology. Compared to its predecessor, 4G long term evolution (LTE) cellular networks, 5G ensures all the usage scenarios and applications of ultrareliable and low latency communications, enhanced mobile broadband, and massive machine-type communications which were envisaged by the International Telecommunication Union Radiocommunication Sector in 2015 [1]. In 2017, it was recognized that a rapid and huge increase in the wireless data traffic volume could be compensated by the spectrum allocation of 5G networks from 0.5 GHz up to 100 GHz [2]. This spectrum is defined as the sub-6-GHz and the mmWave frequency bands. The Citizens Broadband Radio Service which is centered around 3.5 GHz [3] and 4G LTE services also fall into the sub-6-GHz 5G band. The regional spectrum allocation of the mmWave 5G band, however, depends on specific policies of local governments, which makes the band unique. 24–28.5 GHz, 31–33 GHz, and 37–40.5 GHz bands are among the suggested mmWave 5G spectra [4]. Within the spectra, by utilizing any band above 24 GHz, wider channel bandwidths with higher peak data rates than the traditional sub-6-GHz band can be achieved [5–7].

---

*Correspondence: oakgun@dho.edu.tr

This achievement has triggered the recently conducted research and development regarding mmWave band 5G equipment. However, the research in this field should be carried out carefully in terms of propagation such as path loss, blocking, and atmosphere attenuation since these issues become more challenging in mmWave band communications than the lower frequency communication systems [8–10].

Being an indispensable component in a 5G wireless communication system, mmWave antennas have attracted increasing attention over the last years. Various types of 5G mmWave antenna arrays with beam steering capabilities are proposed for cellular handsets [11, 12]. Phased array antennas examining coverage efficiency are also developed [13, 14]. The SIW [15–17] has been widely employed in mmWave circuits such as resonators and filters [18–20]. SIW technology consists of a broad microstrip line having linear arrays of metallic vias at the edges and acts as a rectangular waveguide with dielectric filling. SIW also utilizes its inherent advantages of low loss, low profile, easy manufacturing, and excellent integration with other planar circuits while possessing the benefits of traditional rectangular waveguides. SIW confers its integration capability on mmWave applications in planar antennas. In [21], the leakage loss increasing with the spacing between the vias is used to design periodic leaky-wave antenna whose radiation occurs due to space harmonics of the dominant mode. The circularly polarized dual loop antenna [22] is enclosed by a square SIW cavity with the aim of reducing the surface waves and consequently improving the antenna gain. Unlike these successful designs, it is not misleading to state that horn antennas based on SIW technology are among the most popular ones. In mmWave applications, particularly in those where end-fire radiation is required, SIW horn is considered to be a promising candidate [23, 24]. Compared to conventional horn antennas with bulky and heavy three-dimensional (3D) geometry, the SIW horn possesses all the prominent characteristics of the SIW structure mentioned above. On the other hand, unlike a 3D conventional horn antenna, a SIW horn has a distinct drawback. The dielectric material inside a SIW horn causes reflection of electromagnetic (EM) waves from the boundary of antenna aperture due to the permittivity difference [25]. This discontinuity between the dielectric-filled substrate and the free space results in narrow impedance bandwidth of the planar SIW horn antenna. To overcome this drawback, dielectric lenses at the front of horn apertures are proposed for improving impedance matching [26, 27]. Based on this proposal, a modified dielectric slab, obtained by drilling air-vias having different diameters [25], is used to enhance the impedance bandwidth of the SIW horn. The performance of lens-corrected SIW horns is restricted by the substrate thickness since the effect of a dielectric lens is negligible for a thickness of less than $\lambda_0/6$. As the substrate gets thinner, the beamwidth increases and the FTBR decreases [28]. An alternative solution is to utilize printed transitions. In [28, 29], a printed transition of three parallel-plate blocks is proposed. However, each block has a length of almost $0.25\lambda_0$, causing an increase in the total horn length. To decrease the effective permittivity of the parallel-plate blocks, gratings are added along the transversal direction [30]. In this case, there is a trade-off between the reflection coefficient and the FTBR. In a recent study [31], rectangular patches are loaded in front of the aperture to broaden the bandwidth of a SIW H-plane horn antenna. With the help of slow-wave structures inside the flared region of the horn, a gain enhancement of 1.1 dBi on average is achieved over the 27.5–28.5 GHz band.

This study presents an H-plane SIW horn antenna with printed transitions at the front of the horn aperture. The purpose of the printed transitions is to reduce the matching and radiation problems caused by the SIW horn being printed onto an electrically thin substrate. In particular, the printed transitions are adapted to enhance the FTBR of the SIW horn. In Section 2, we introduce the geometries and the design parameters of the H-plane SIW horn antennas. Section 3 provides the performance analysis of the proposed SIW horns based on simulation results. Section 4 is dedicated to experimental verification.

2. H-plane SIW horn antenna

A conventional 3D horn antenna is a rectangular waveguide having different cross sections along the horn's length. Flaring the waveguide dimension that is parallel to the H-field and keeping the perpendicular one constant creates the radiation in the H-plane, consequently forming an H-plane sectoral horn. In this study, using the advantage of planar SIW, an H-plane sectoral horn antenna, operating in the 24–28 GHz band, is converted to an H-plane SIW horn antenna. The substrate of the planar horn is chosen as Rogers 5870 ($\varepsilon_r = 2.33$ and $\tan \delta = 0.0011$ at 28 GHz) with $h_d = 1.57$ mm dielectric thickness and 35 μm copper cladding. When the H-plane sectoral horn is transformed into its planar version, a high reflection occurs at the dielectric-free space boundary. Thus, IMTs are proposed for the transition from the planar horn aperture to the free space. Detailed information on the antennas and impedance matching sections are demonstrated in the following subsections.

2.1. SIW horn antenna design

H-plane SIW horn antenna is given in Figure 1. It consists of two parts: the microstrip tapered feed and the SIW horn. A 50 Ω microstrip line is used to feed the SIW horn. A tapered transition between the microstrip line and the SIW is used. For the SIW part of the antenna, we start with a mono-mode SIW structure. The structure aims to suppress the higher-order waveguide modes entirely and support the propagation of the fundamental TE_{10} mode. To obtain the parameters of the SIW, we use the design rules of [17], particularly $p/d < 2$ and $d/W < 0.2$, where p is the pitch distance between the centers of two adjacent vias, and d is the diameter of a metallic via. The width $W = 8.4$ mm, measured from the centers of via walls, is calculated by solving the well-known empirical equation in [16]. At the flaring, we continue with the tapered metallic vias up to the radiating aperture of width, W_h. The final dimensions of the H-plane SIW horn that are obtained considering fabrication constraints are given in Table 1.
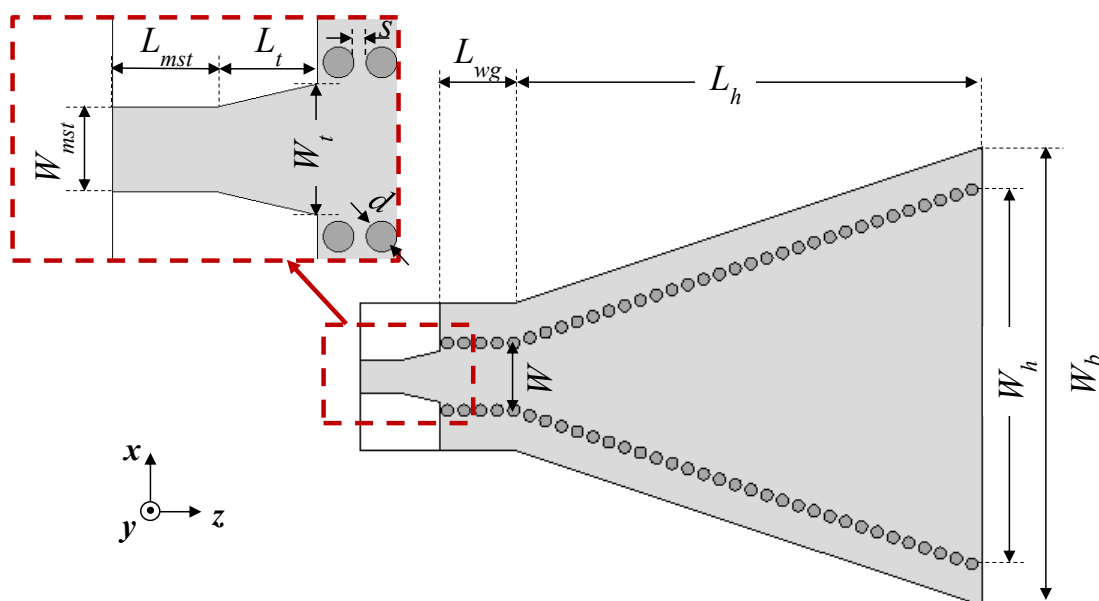

Figure 1. Microstrip fed H-plane SIW horn antenna. Details of the feedline is exhibited in the inset with its parameters.

The radiation characteristics of the antenna in Figure 1 can be found when the tangential electric and magnetic field components over the aperture's surface are known. The aperture acts as a radial waveguide [32] which enables us to find the field components. The related mathematical expressions of the aperture fields are similar to those of the TE mode of a dielectric-filled rectangular waveguide with aperture dimensions of W_h and h_d. However, due to the phase variations of the aperture fields, there should be an additional complex-valued exponential term. The exponent includes the phase error, $\delta(x)$, which occurs because of the path difference to be traveled by the wave from the imaginary apex of the horn to any point on the aperture surface [33]. An easy solution to decrease $\delta(x)$ is to minimize the flare angle. Due to the mono-mode SIW structure of the horn antenna, the electric field distribution at the aperture, E_{ap}, is proportional to $cos(\pi x/W_h)$. In [30], with the motivation of obtaining more uniform electric field distribution at the aperture, TE_{10} and TE_{30} modes are combined. It is also explained in [30] that instead of a mono-mode waveguide, a coaxial feed or a multilayer transition is required to excite both modes. Consequently, the authors in [30] propose an elliptical horn taper with coaxial feeding. In our study, the mono-mode SIW structure is chosen intentionally to guarantee the dominant TE_{10} mode.

Table 1. Dimensions of the H-plane SIW horn antenna (all units are in mm)

SIW horn antenna		Feedline		Impedance matching transition	
W_b	58	W_{mst}	4.1	L_{tr}	2.75
W_h	47.4	L_{mst}	5	W_{tr}	1.39
L_h	59	W_t	6.4	g	0.25
s	0.45	L_t	5	g'	0.25
d	1.65	L_{wg}	9.45	s'	0.5

2.2. SIW horn antenna with triangular impedance matching transitions

To our knowledge, the most comprehensive work on IMTs applied to a planar SIW horn's aperture belongs to Esquius-Morote et al. Their work aims to reduce the impedance mismatch, decreasing operational bandwidth, between a thin-substrate horn aperture and the free space. For this purpose, a printed transition of concatenated monolithic rectangular blocks was introduced in [28], where two different models are given for the proposed transition. In the first, Esquius-Morote et al. treated the blocks as coupled resonators since each block is a parallel plate waveguide separated by dielectric gaps. As a second case, they considered the printed transition as blocks of a transmission line whose primary propagating mode is the transverse electromagnetic mode. While the proposed transition effectively improved the operational bandwidth, it caused no amendment in the radiation characteristics of the antenna. Thus, the transition resulted in a low FTBR, particularly below 5 dB [28]. In a later work [30], they reconsidered the transition design from the radiation point of view and modified it to improve the FTBR. As the first step, they used grated structures with a rectangular pattern rather than a monolithic rectangular block. Since there are dielectric gaps between each metallic grating structure, the effective permittivity of the dielectric substrate, ε_{eff}, gained importance in the design process. Due to a change in the value of ε_{eff} and the noncontinuous metallic surface at the horn aperture, the field distribution became less uniform in the SIW horn antenna, which resulted in a slightly wider beamwidth. With the motivation of controlling this effect, they proposed nonuniform gratings. The shape of the rectangular gratings was tapered, yielding to triangular gratings.

Before investigating the novel design of the proposed printed transition, we explain the initial steps in the following. To design the printed transition having triangular impedance matching elements in Figure 2a, we start with determining an element's length that maximizes the FTBR. The length of the triangular impedance matching elements is calculated from

$$L_{tr} = \frac{c}{2\,f_{FTBR}\left(1 + \sqrt{0.5\,\varepsilon_{eff}}\right)},$$
(1)

where c is the speed of light in vacuum, and ε_{eff} denotes the effective permittivity obtained from the quasistatic approximation given in [34]. The parameter f_{FTBR} at the denominator of (1) is the frequency at which the FTBR is maximum. Figure 2b demonstrates the variation of the ε_{eff} value as the function of frequency aiming to increase the FTBR. Consequently, for the value of $\varepsilon_{eff} \approx 2$, the length of the triangular impedance matching elements is calculated as $L_{tr} = 2.75$ mm at the frequency of 27 GHz that maximizes the FTBR.
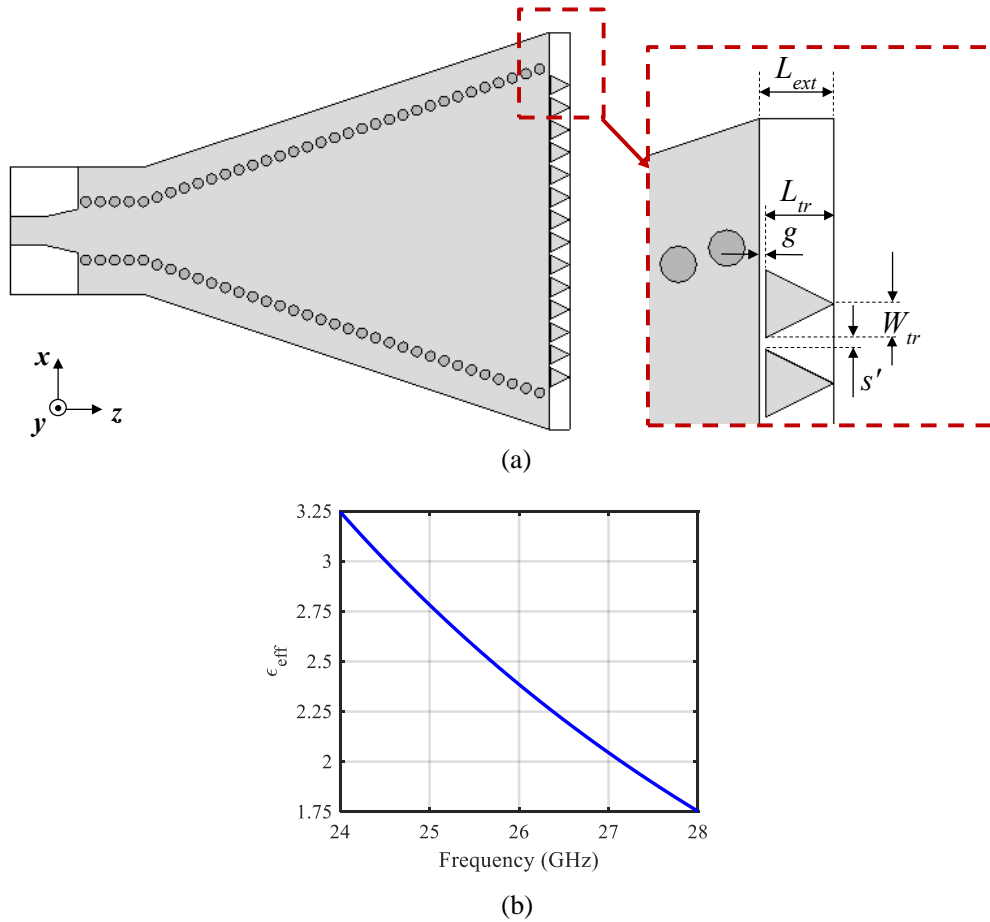

Figure 2. (a) H-plane SIW horn antenna with triangular impedance matching transitions. Details of the triangular elements are exhibited in the inset with their relating parameters. (b) The effective permittivity as the function of frequency.

Next, we continue with the full-wave simulations to determine the optimum value for the gap, g. Optimization constraints are the main lobe magnitude (MLM), the SLL, the FTBR, and the 3 dB angular

width. The values regarding the constraints are obtained at 27 GHz since the length L_{tr} is calculated at this frequency. The worst-case belongs to $g = 0$ mm, where there is no gap between the horn's aperture and the triangular impedance matching elements. In terms of MLM, the performances of $g = 0.25$ mm and $g = 0.4$ mm are close to each other. However, the SLL and the FTBR values of $g = 0.25$ mm are far better than those of $g = 0.4$ mm. Besides, $g = 0.25$ mm has the advantage of narrower 3 dB angular width. As another design guideline, keeping the spacing s' small enough is necessary not to encounter undesired radiation, hence, $s' < W_{tr}$. The periodicity of triangular elements, measured from the vertices of two adjacent triangles, should be less than $W_h/10$.

The optimization procedure described above provides a first step before investigating the novel design of printed transition in the following subsection.

2.3. SIW horn antenna with dual-triangle impedance matching transitions

Regardless of their topologies, Esquius-Morote et al. sequenced the printed transitions as blocks of the same pattern cascaded one after another and called them concatenated blocks. The array analogy of the transitions [30] resulted in the improved FTBR of the H-plane SIW horn antenna. Our work suggests a novel dual-triangle structure so that each pair of dual triangles forms an array in a single IMT block. In the structure, we deploy additional triangular elements to the gaps between the previous ones, with the bases of the former and the latter metallic triangles parallel. In other words, we have evaluated the spacing that is already present in a single block without the need to cascade another. The miniaturized structure and lightness of the proposed transition allow us to maintain the most elegant feature of the SIW technology, compactness. With a two-block triangular printed transition, the work in [30] achieves an FTBR value of better than 15 dB. In our case, we obtain an enhanced FTBR of 25.77 dB with a single-block dual-triangle printed transition.

The dual-triangle IMT is used to obtain an enhanced smoothness in the impedance difference between the aperture and the free space. Simulation results of a SIW waveguide with exact horn aperture size show that the wave impedance calculated at 26 GHz, the center frequency of 24–28 GHz band, is almost 248 Ohm at the H-plane horn's aperture. Thus, we can conclude that the dual-triangle IMT converts the aperture impedance to the free-space intrinsic impedance.

The novel pattern of the dual-triangle transition is shown in the inset of Figure 3 together with the parameter g', the separation between the dual-triangle. The other parameters are all identical to the ones in Figure 2a. For simplicity, g' is chosen equal to the parameter, g in the previous design. When the value of g' increases, the effective permittivity, ε_{eff}, evidently decreases. Nevertheless, keeping g' reasonably small has two reasons: to prevent undesired radiation, as explained in the previous subsection. The second reason is to create an impact that the whole impedance-matching layer block works as a quasirectangular parallel plate resonator with an enhanced capacitive coupling between the individual dual-triangle elements. This consideration enables us to explain the working principle of the quasirectangular block theoretically and leads to the resonance frequency formula [35], namely

$$f_{res} = \frac{c}{2\left(L_{tr} + 2\,\Delta L\right)\sqrt{\varepsilon_{eff}}}. \tag{2}$$

In (2), ΔL contributes to the equivalent length of L_{tr} that should be considered due to the fringing fields.

Finally, ε_{eff} is the effective permittivity as

$$\varepsilon_{eff} = \frac{\varepsilon_r + 1}{2} + \frac{\varepsilon_r - 1}{2}\left(1 + 10\,\frac{h_d}{W_h}\right)^{-0.5},\tag{3}$$

where ε_r is the relative permittivity and h_d is the dielectric thickness of the substrate. W_h is the aperture width of the SIW horn antenna.
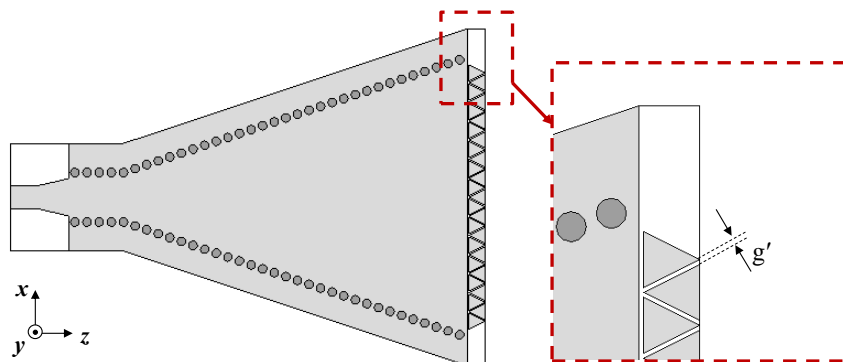

Figure 3. H-plane SIW horn antenna with dual-triangle impedance matching transitions.

3. Performance analysis of H-plane SIW horn antennas

We observe the performances of H-plane SIW horn antennas using a full-wave EM simulator, CST Microwave Studio, where the analyses are carried out in the time-domain solver. We demonstrate the reflection coefficient, S_{11}, of the three antennas in Figure 4. It is observed that S_{11} of the antenna without IMT hardly goes below –10 dB. The effect of adding IMTs to the antenna/free space interface is clearly observed in the figure. With triangular IMT, the antenna's bandwidth extends to 25–32 GHz, whereas it becomes wider for IMT with dual triangles which is 23.5–31.5 GHz. In Figure 5a, we compare the realized gain of the three H-plane SIW horn antennas as the function of frequency. The realized gain of an antenna depends on the parameters of directivity and reflection coefficient [24]. Once reflection from the antenna/free space interface is reduced by the IMTs, an enhancement in the gain values is observed in the figure. For instance, at 27 GHz, the novel design of IMT with dual triangles has a gain value of better than 9 dBi. In the whole frequency band, a gain enhancement up to 4 dBi is obtained by the IMT with dual triangles. In the 24–28 GHz band, the total efficiency of the antenna with dual-triangle IMT varies from 0.85 up to 0.9, whereas that of antenna with triangular IMT is between 0.78 and 0.88. When the antenna does not have an IMT, the efficiency values are in the 0.45–0.7 range, as shown in Figure 5a.

Figure 5b exhibits the FTBR variation of the three H-plane SIW horn antennas as the function of frequency. Although the antennas with IMTs show a similar FTBR characteristic, the one with dual-triangle IMT has better FTBR values. With the dual-triangle IMT, we aimed to obtain high FTBR values over a wide impedance bandwidth, 24–28 GHz. The design considerations of the IMTs are based on the specific frequency of 27 GHz that maximizes the FTBR in the band. The FTBR behavior of the dual-triangle IMT at 28 GHz is very close to that at 27 GHz, see Figure 5b. The FTBR is reasonable at 24 GHz though worse than the one at 27 GHz. Besides, Figure 5b proves that the FTBR is maximal at 27 GHz.
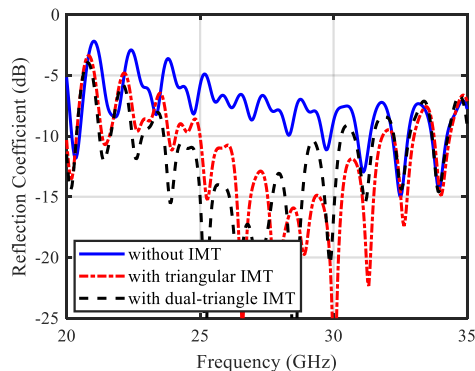
Figure 4. Reflection coefficient variation of the H-plane SIW horn antennas.
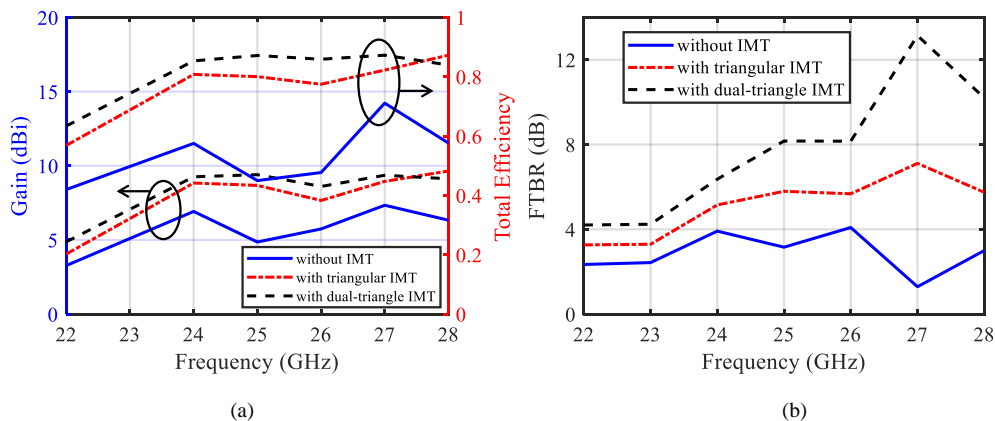

Figure 5. (a) Gain and total efficiency variations of the H-plane SIW horn antennas. The left scale demonstrates the gain, whereas the right scale demonstrates the total efficiency. (b) The FTBR variation of the H-plane SIW horn antennas.

Figure 6 compares the normalized radiation patterns of the H-plane SIW horn antennas regarding IMTs in $\phi = 0\,°$ plane. At 24 GHz, 3 dB beamwidths of the three SIW horns are almost equal. The unmatched antenna has an FTBR value of 3.9 dB at this frequency, while the IMT with dual triangles has improved the FTBR value up to 2.5 dB. The H-plane horn antenna without IMT has a high SLL value at 26 GHz. Like an all-metallic 3D horn antenna, the conventional H-plane SIW horn has a high SSL value attributed to the edge-diffracted fields. These diffractions strongly distort radiation which causes poor radiation characteristics such as high SLL and low FTBR. At 26 GHz, the SLL values of the antennas with IMTs are much more favorable than that without IMT. This fact may be the reason for the high SLL of the H-plane horn antenna without IMT. Moreover, the FTBR enhancement with dual-triangle IMT is more than 7 dB at 28 GHz compared to the one without IMT. Unlike the general antenna structures, the beamwidth of the H-plane SIW horns in $\phi = 0\,°$ plane widens with increasing frequency. Radiation patterns of this plane have narrow beamwidths due to the wide aperture width at the x-z plane. However, the narrow thickness of the aperture in the y-z plane ($\phi = 90\,°$ plane) generates broad radiation patterns, as shown in Figure 7.
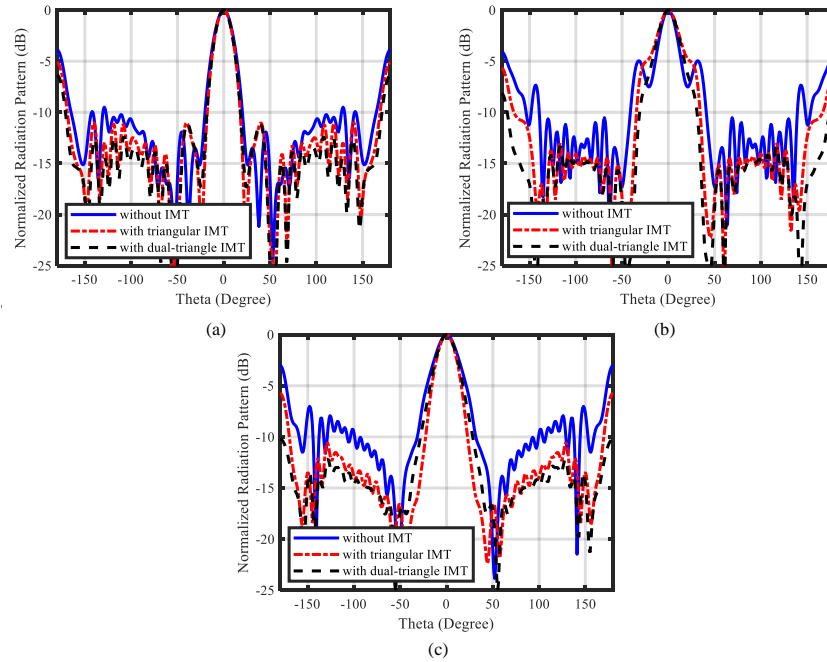
Figure 6. Normalized radiation patterns of the H-plane SIW horn antennas with impedance matching transitions in $\phi = 0\,^{\circ}$ plane (a) 24 GHz, (b) 26 GHz, (c) 28 GHz.

Figure 7. Normalized radiation patterns of the H-plane SIW horn antennas with impedance matching transitions in $\phi = 90\,^{\circ}$ plane (a) 24 GHz, (b) 26 GHz, (c) 28 GHz.
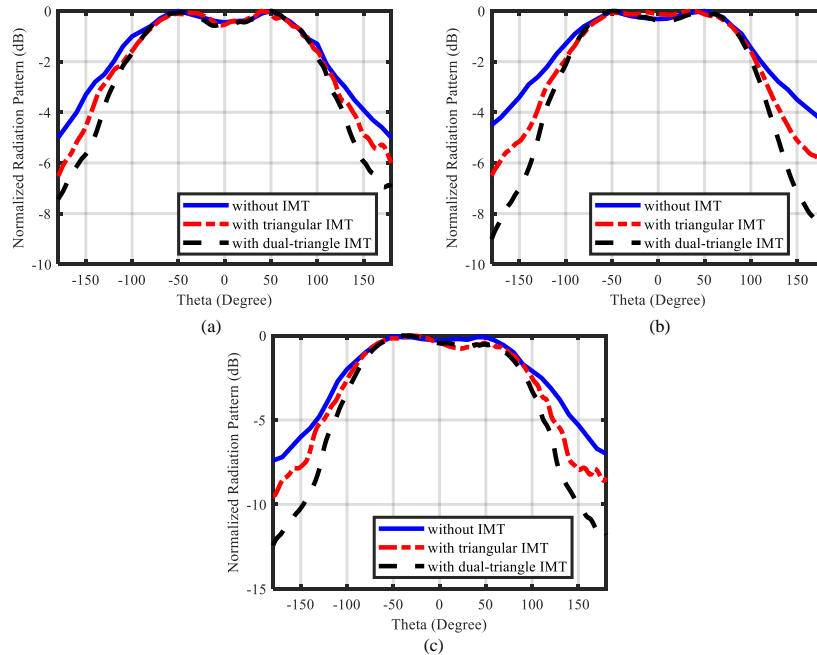
4. Experimental verification

Three prototypes of H-plane SIW horn antennas in Figure 8 have been designed, fabricated, and measured to validate the advantages of the proposed IMT. Rogers RT/Duroid 5870 $\varepsilon_r = 2.33$ laminate with a dielectric thickness of $h_d = 1.57$ mm and a copper cladding of 35 μm is used in the fabrication process. A tapered microstrip line is designed for transition from the connector to the SIW structure. A 50 Ω Pasternack SMA (SubMiniature version A) connector operating up to 27 GHz with an insertion loss of 0.26 dB is used to feed the SIW horn. Figure 9 shows the measured reflection coefficient of the antennas. As can be seen from the figure, the lowest reflection coefficient variation is obtained for the H-plane SIW horn antenna with a novel IMT design with dual triangles, where it is below –10 dB in the 24.5–28 GHz frequency band.
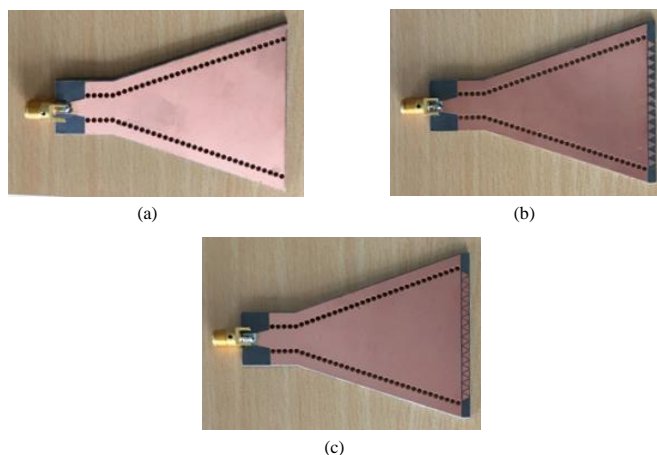

(a) (b)

(c)

Figure 8. Fabricated H-plane SIW horn antenna prototypes (a) without IMT, (b) with triangular IMT, (c) with dual-triangle IMT.

In Figure 10, we compare the copolarized, normalized radiation patterns of the three H-plane SIW horn antennas in $\phi = 0\,^\circ$ and $\phi = 90\,^\circ$ planes, particularly at 24 GHz and 27 GHz. Similar to the simulation results, beamwidths of the patterns at 24 GHz are narrower than those at 27 GHz. At 24 GHz, the 3 dB beamwidth of the SIW horns is very close to one another, which complies with the simulation results. In $\phi = 0\,^\circ$ plane, especially for the antenna without IMT, the SLLs are slightly higher than the simulation results. The disagreement is attributed to the nonideal, real-world measurement setup. SLLs of the antennas with IMTs partly go above –10 dB. However, since the values are still below –9 dB, they can be considered acceptable. Besides, we propose the H-plane SIW horn antenna with dual-triangle IMT for specific applications at a base station side. In a base station terminal, the antennas are widely used in an array form. This type of usage of the proposed antenna would reduce the SLL level. The FTBR of the SIW horn without IMT is 7.63 dB and 9.83 dB at 24 and 27 GHz, respectively. These values increase to 15.32 dB and 15.89 dB, respectively, when the IMT with triangles is included. The FTBR even increases more with the dual-triangle IMT. Thus, an enhancement of the FTBR is clearly observed with the SIW horn having the novel design of dual-triangle IMT. Similar FTBRs are obtained in $\phi = 90\,^\circ$ plane with the simulation results. The FTBR of the SIW horn with dual-triangle IMT is higher than that of the SIW horn with triangular IMT at both 24 and 27 GHz.

Table 2 presents comparisons of the proposed antenna with other H-plane SIW horn antennas. The proposed SIW horn features an improved FTBR level and a wide fractional bandwidth thanks to the dual-triangle IMTs.
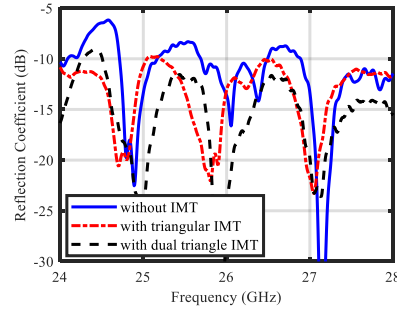
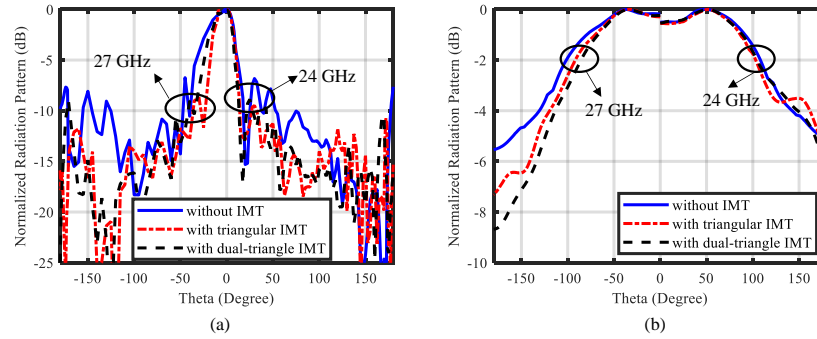**Figure 9**. Measured reflection coefficient of the H-plane SIW horn antennas.

Figure 10. Measured normalized radiation patterns of the H-plane SIW horn antennas (a) $\phi = 0\,^\circ$ plane, (b) $\phi = 90\,^\circ$ plane.

Table 2. Comparison of H-plane SIW horn antennas.

Ref.	Structure		Freq. [GHz]	Fr. BW (%)	Gain [dBi]	FTBR [dB]	Size [$\lambda_0 \times \lambda_0 \times \lambda_0$]
[24]	Gap SIW with triangular IMT		34	20	10.3	10[a]	4.40x2.30x0.17
[28]	Conv. SIW with rectangular IMT	1 block	14.7	8.2	n.a.[b]	3-4	1.3x1.07x0.09[c]
		2 blocks	12.2	4.5	n.a.[b]	3-4	1.60x1.10x0.08[c]
		3 blocks	14.4 & 17.3	9.8 & 4.3	n.a.[b]	n.a.[b]	1.7x1.05x0.09[c]
[30]	Elliptical SIW with a two-block triangular IMT		14.8	10.4	7.1	>15	1.56x1.26x0.09
[31]	Conv. SIW with rectangular IMT and blind via-holes		28	10.71	>5	n.a.[b]	2.24x2.78x0.14[c]
Proposed	Conv. SIW with a single-block dual-triangle IMT		27	13.3	9.36[a]	>15	5.6x4.26x0.14[c]

[a]Simulated result.

[b]Not available.

[c]Without mono-mode SIW and feeding line.

5. Conclusion

A modified, low-profile H-plane SIW horn antenna with a novel printed transition section is designed mainly for mmWave 5G applications. Simulated and measured results have shown that the IMT positively affects the reflection at the antenna aperture/free space interface. The antenna operates with a low reflection coefficient in the 24–28 GHz band. Once the reflection from the interface is prevented with dual-triangle IMT, an excellent FTBR is achieved. With the advantages of integration capability, low profile, and high FTBR, the H-plane SIW horn antenna with dual-triangle IMT may be considered an excellent choice for specific applications at the base station side in the mmWave frequency bands.

References

[1] IMT vision – framework and overall objectives of the future development of IMT for 2020 and beyond. Document Rec. ITU-R M.2083-0, ITU-R, Geneva, Switzerland, September 2015.

[2] Study on channel model for frequencies from 0.5 to 100 GHz. Technical Report, 3GPP TR 138.901 V14.0.0, Release 14, May 2017.

[3] Amendment of the commission's rules with regard to commercial operations in the 3550–3650 MHz band. Federal Communications Commission, 47 CFR Part 96, June 2017.

[4] Hong W. Solving the 5G mobile antenna puzzle: Assessing future directions for the 5G mobile antenna paradigm shift. IEEE Microwave Magazine 2017; 18 (7): 86-102. doi: 10.1109/MMM.2017.2740538

[5] Lota J, Sun S, Rappaport TS, Demosthenous A. 5G uniform linear arrays with beamforming and spatial multiplexing at 28, 37, 64, and 71 GHz for outdoor urban communication: A two-level approach. IEEE Transactions on Vehicular Technology 2017; 66 (11): 9972-9985. doi: 10.1109/TVT.2017.2741260

[6] Xu B, Ying Z, Scialacqua L, Scannavini A, Foged LJ et al. Radiation performance analysis of 28 GHz antennas integrated in 5G mobile terminal housing. IEEE Access 2018; 6: 48088-48101. doi: 10.1109/ACCESS.2018.2867719

[7] Taheri MMS, Abdipour A, Zhang S, Pedersen GF. Integrated millimeter-wave wideband end-fire 5G beam steerable array and low-frequency 4G LTE antenna in mobile terminals. IEEE Transactions on Vehicular Technology 2019; 68 (4): 4042-4046. doi: 10.1109/TVT.2019.2899178

[8] MacCartney GR, Rappaport TS, Sun S, Deng S. Indoor office wideband millimeter-wave propagation measurements and channel models at 28 GHz and 73 GHz for ultra-dense 5G wireless networks. IEEE Access 2015; 3: 2388–2424. doi: 10.1109/ACCESS.2015.2486778

[9] Ferrante S, Pietraski P, Deng T, Bielinski M. mm Wave UE antenna configuration study. In: IEEE 2015 81st Vehicular Technology Conference; Glasgow, Scotland, UK; 2015. pp. 1-6.

[10] Sun S, MacCartney GR, Rappaport TS. Millimeter-wave distance-dependent large-scale propagation measurements and path loss models for outdoor and indoor 5G systems. In: 2016 The 10th European Conference on Antennas and Propagation; Davos, Switzerland; 2016. pp. 1-6.

[11] Yu B, Yang K, Sim CYD, Yang G. A novel 28 GHz beam steering array for 5G mobile device with metallic casing application. IEEE Transactions on Antennas and Propagation 2018; 66 (1): 462-466. doi: 10.1109/TAP.2017.2772084

[12] Ozpinar H, Aksimsek S, Turker Tokan N. A novel compact, broadband, high gain millimeter-wave antenna for 5G beam steering applications. IEEE Transactions on Vehicular Technology 2020; 69 (3): 2389-2397. doi: 10.1109/TVT.2020.2966009

[13] Helander J, Zhao K, Ying Z, Sjöberg D. Performance analysis of millimeter wave phased array antennas in cellular handsets. IEEE Antennas and Wireless Propagation Letters 2016; 15: 504-507. doi: 10.1109/LAWP.2015.2455040

[14] Zhang S, Chen X, Syrytsin I, Pedersen GF. A planar switchable 3D-coverage phased array antenna and its user effects for 28 GHz mobile terminal applications. IEEE Transactions on Antennas and Propagation 2017; 65 (12): 6413–6421. doi: 10.1109/TAP.2017.2681463

[15] Deslandes D, Wu K. Integrated transition of coplanar to rectangular waveguides. In: IEEE 2001 MTT-S International Microwave Symposium Digest; Phoenix, AZ, USA; 2001. pp. 619-622.

[16] Cassivi Y, Perregrini L, Arcioni P, Bressan M, Wu K et al. Dispersion characteristics of substrate integrated rectangular waveguide. IEEE Microwave Wireless Components Letters 2002; 12 (9): 333–335. doi: 10.1109/LMWC.2002.803188

[17] Xu F, Wu K. Guided-wave and leakage characteristics of substrate integrated waveguide. IEEE Transactions on Microwave Theory and Techniques 2005; 53 (1): 66-73. doi: 10.1109/TMTT.2004.839303

[18] Deslandes D, Wu K. Single-substrate integration technique of planar circuits and waveguide filters. IEEE Transactions on Microwave Theory and Techniques 2003; 51 (2): 593–596. doi: 10.1109/TMTT.2002.807820

[19] Lee GH, Yoo CS, Kim YH, Kim JY, Park YH et al. A 60 GHz embedded SIW (substrate integrated waveguide) BPF considering the transition effect. In: 2009 Asia Pacific Microwave Conference; Singapore; 2009. pp. 1192-1195.

[20] Zhu Y, Chen J, Yan P. Millimeter-wave band-pass filter based on complementary split ring and SIW resonators. In: 2015 Asia Pacific Microwave Conference; Nanjing, China; 2015. pp. 1-3.

[21] Xu F, Wu K, Zhang X. Periodic leaky-wave antenna for millimeter wave applications based on substrate integrated waveguide. IEEE Transactions on Antennas and Propagation 2010; 58 (2): 340-347. doi: 10.1109/TAP.2009.2026593

[22] Mei H, Yang X, Yu Y. SIW cavity-backed circularly polarized dual loop antenna with broadband at Ka band. In: 2016 International Symposium on Antennas and Propagation; Okinawa, Japan; 2016. pp. 710-711.

[23] Zhang YX, Jiao YC, Zhang L. Wideband inhomogeneous-polarizer loaded circularly polarized SIW horn antenna for broadband millimeter-wave applications. IEEE Antennas and Wireless Propagation Letters 2019; 18 (7): 1448-1452. doi: 10.1109/LAWP.2019.2919636

[24] Wang L, Esquius-Morote M, Qi H, Yin X, Mosig JR. Phase corrected H-plane horn antenna in gap SIW technology. IEEE Transactions on Antennas and Propagation 2017; 65 (1): 347-353. doi: 10.1109/TAP.2016.2623656

[25] Cai Y, Qian ZP, Zhang YS, Jin J, Cao WQ. Bandwidth enhancement of SIW horn antenna loaded with air-via perforated dielectric slab. IEEE Antennas and Wireless Propagation Letters 2014; 13: 571-574. doi: 10.1109/LAWP.2014.2312917

[26] Che W, Fu B, Yao P, Chow YL, Yung EKN. A compact substrate integrated waveguide H-plane horn antenna with dielectric arc lens. International Journal of RF and Microwave Computer-Aided Engineering 2007; 17 (5): 473-479. doi: 10.1002/MMCE.20237

[27] Wang J, Li Y, Wang J. Wideband dipole array loaded substrate-integrated horn array with improved sidelobe performance. IEEE Antennas and Wireless Propagation Letters 2019; 18 (3): 556-560. doi: 10.1109/LAWP.2019.2896600

[28] Esquius-Morote M, Fuchs B, Zürcher JF, Mosig JR. A printed transition for matching improvement of SIW horn antennas. IEEE Transactions on Antennas and Propagation 2013; 61 (4): 1923-1930. doi: 10.1109/TAP.2012.2231923

[29] Esquius-Morote M, Fuchs B, Mosig JR. Analytical model of a printed transition for SIW antennas. 2012 6th European Conference on Antennas and Propagation; Prague, Czech Republic; 2012. pp. 414-417.

[30] Esquius-Morote M, Fuchs B, Zürcher JF, Mosig JR. Novel thin and compact H-plane SIW horn antenna. IEEE Transactions on Antennas and Propagation 2013; 61 (6): 2911-2920. doi: 10.1109/TAP.2013.2254449

[31] Zhang Y. Deng JY, Sun D, Yin JY, Guo LX. Compact slow-wave SIW H-plane horn antenna with increased gain for vehicular millimeter wave communication. IEEE Transactions on Vehicular Technology 2021; 70 (7): 7289-7293. doi: 10.1109/TVT.2021.3090096

[32] Balanis CA. Advanced Engineering Electromagnetics. New York, USA: Wiley, 2012.

[33] Balanis CA. Antenna Theory: Analysis and Design. New York, USA: Wiley, 2005.

[34] Benedek P, Silvester P. Capacitance of parallel rectangular plates separated by a dielectric sheet. IEEE Transactions on Microwave Theory and Techniques 1972; 20 (8): 504–510. doi: 10.1109/TMTT.1972.1127797

[35] Yazdandoost KY, Gharpure DC. Simple formula for calculation of the resonant frequency of a rectangular microstrip antenna. In: IEEE 1998 5th International Symposium on Spread Spectrum Techniques and Applications; Sun City, South Africa; 1998. pp. 604-605.